J|A|C|S
ARTICLES
Published on Web 05/16/2006

Ytterbocene Charge-Transfer Molecular Wire Complexes

Christin N. Carlson, Christopher J. Kuehl, Ryan E. Da Re, Jacqueline M. Veauthier, Eric J. Schelter, Ashley E. Milligan, Brian L. Scott, Eric D. Bauer, J. D. Thompson, David E. Morris,* and Kevin D. John*

Contribution from the Chemistry and Materials Science Divisions, Los Alamos National Laboratory, Los Alamos, New Mexico 87545

Received December 21, 2005; E-mail: kjohn@lanl.gov; demorris@lanl.gov

Abstract: A systematic study of the novel charge-transfer [$(f)^{14}$-$(\pi^*)^0$-$(f)^{14} \rightarrow (f)^{13}$-$(\pi^*)^2$-$(f)^{13}$] electronic state found in 2:1 metal-to-ligand adducts of the type [$(Cp^*)_2Yb$](BL)[$Yb(Cp^*)_2$] [BL = tetra(2-pyridyl)pyrazine (tppz) (**1**), 6′,6″-bis(2-pyridyl)-2,2′:4′,4″:2″,2‴-quaterpyridine (qtp) (**2**), 1,4-di(terpyridyl)-benzene (dtb) (**3**), $Cp^* = (C_5Me_5)$] has been conducted with the aim of determining the effects of increased Yb−Yb separation on the magnetic and electronic properties of these materials. The neutral [$(f)^{13}$-$(\pi^*)^2$-$(f)^{13}$], cationic [$(f)^{13}$-$(\pi^*)^1$-$(f)^{13}$] and dicationic [$(f)^{13}$-$(\pi^*)^0$-$(f)^{13}$] states of these complexes were studied by cyclic voltammetry, UV−vis−NIR electronic absorption spectroscopy, NMR, X-ray crystallography, and magnetic susceptibility measurements. The spectroscopic and magnetic data for the neutral bimetallic complexes is consistent with an [$(f)^{13}(\pi^*)^2(f)^{13}$] ground-state electronic configuration in which each ytterbocene fragment donates one electron to give a singlet dianionic bridging ligand with two paramagnetic Yb(III) centers. The voltammetric data demonstrate that the electronic interaction in the neutral molecular wires **1**−**3**, as manifested in the separation between successive metal reduction waves, is large compared to analogous transition metal systems. Electronic spectra for the neutral and monocationic bimetallic species are dominated by $\pi-\pi^*$ and $\pi^*-\pi^*$ transitions, masking the f−f bands that are expected to best reflect the electronic metal−metal interactions. However, these metal-localized transitions are observed when the electrons are removed from the bridging ligand via chemical oxidation to yield the dicationic species, and they suggest very little electronic interaction between metal centers in the absence of π^* electrons on the bridging ligands. Analysis of the magnetic data reveals that the qtp complex displays antiferromagnetic coupling of the type Yb(α)($\alpha\beta$)Yb(β) at ~13 K.

Introduction

A stable charge-transfer electronic configuration [$(f)^{14}$-$(\pi^*)^0 \rightarrow (f)^{13}$-$(\pi^*)^1$] has recently been reported for a range of N-heterocyclic base adducts of ytterbocene (e.g., $Cp^*_2Yb(L)$: $Cp^* = C_5Me_5$; L = 2,2′-bipyridine (bpy), 1,10-phenanthroline (phen), 2,2′;6′,2″-terpyridine (tpy), 4′-cyano-2,2′:6′,2″:-terpyridine (tpy-CN)).[1−5] This electronic state derives from a spontaneous electron transfer from the diamagnetic f^{14} Yb(II) metal center (donor) to the lowest unoccupied molecular orbital (LUMO) on the N-heterocyclic ligand (acceptor), which gives rise to a paramagnetic species involving an f^{13} metal center and a ligand radical anion. A similar phenomenon has been observed for many 2:1 ytterbocene-bridging polypyridyl adducts in which the bridging N-heterocyclic ligand is doubly reduced (one electron from each metal center) with the two electrons reported to reside in a spin-paired configuration in the same LUMO.[3,5a]

Our interest in this charge-transfer phenomenon, at least in part, has been sparked by a desire to create new model systems for molecular electronic and nanoscale devices (e.g., molecular wires). There is a strong analogy between these bimetallic ytterbocene structures and the more familiar transition-metal bimetallic systems such as the widely studied Creutz-Taube ion.[6] In particular, the electronic structures of these stable charge-transfer states in the ytterbocene complexes (i.e., oxidized metal and reduced ligand) are analogous to the *excited* electronic states in d^6 transition-metal polypyridyl complexes such as the well-characterized $[Ru(bpy)_3]^{2+}$, which have demonstrated potential for a variety of applications such as photovoltaic and electrochromic devices.[7] Furthermore, the ytterbocene charge-transfer

(1) Da Re, R. E.; Kuehl, C. J.; Brown, M. G.; Rocha, R. C.; Bauer, E. D.; John, K. D.; Morris, D. E.; Shreve, A. P.; Sarrao, J. L. *Inorg. Chem.* **2003**, *42*, 5551.
(2) Veauthier, J. M.; Schelter, E. J.; Kuehl, C. J.; Clark, A. E.; Scott, B. L.; Morris, D. E.; Martin, R. L.; Thompson, J. D.; Kiplinger, J. L.; John, K. D. *Inorg. Chem.* **2005**, *44*, 5911.
(3) Berg, D. J.; Boncella, J. M.; Andersen, R. A. *Organometallics* **2002**, *21*, 4622.
(4) Schultz, M.; Boncella, J. M.; Berg, D. J.; Tilley, T. D.; Andersen, R. A. *Organometallics* **2002**, *21*, 460.
(5) (a) Kuehl, C. J.; Da Re, R. E.; Scott, B. L.; Morris, D. E.; John, K. D. *Chem. Commun.* **2003**, 2336. (b) Da Re, R. E.; Kuehl, C. J.; Donohoe, R. J.; John, K. D.; Morris, D. E. *Electronic Spectroscopy of [$(C_5Me_5)_2Yb(L)]^+$ (L = 2,2′-bipyridine and 2,2′:6′,2″-terpyridine). Vibronic Coupling and Ligand-field Splitting in the $4f^{13}$-Derived Ground and Excited States of Yb^{3+}*; Los Alamos National Laboratory: Los Alamos, NM, 2005; LA-UR-05-5249.
(6) Kaim, W.; Klein, A.; Glockle, M. *Acc. Chem. Res.* **2000**, *33*, 755.
(7) (a) Schanze, K. S.; Walters, K. A. Photinduced electron transfer in metal-organic dyads. In *Molecular and Supramolecular Photochemistry*; Marcel Dekker: New York, 1998; Vol. 2. (b) Balzani, V.; Juris, A.; Venturi, M.; Campanga, S.; Serroni, S. *Chem. Rev.* **1996**, *96*, 759. (c) Ward, M. D. *Chem. Soc. Rev.* **1995**, *34*, 121.

 10.1021/ja058667e CCC: $33.50

complexes are readily manipulated by chemical or electrochemical means, so it is possible to tune the magnetic coupling in these multiple-spin systems. This property is important for applications in the emerging fields of molecular magnetism[8] and spintronics.[9]

Numerous synthetic strategies are available to influence the electron-transfer phenomenon. For example, Andersen and co-workers have modified the substituents on the cyclopentadienyl ligands to increase the electropositivity at the Yb center relative to that in Cp^*_2Yb thereby inhibiting the ground-state electron-transfer process.[4] Similarly, by varying the N-heterocyclic ligand from bidentate to tridentate, it may be possible to establish ligand-based potential energy thresholds for the occurrence of the charge transfer and to categorize ranges of magnetic behavior by altering the energy of the ligand LUMO. The present work was undertaken to explore the influence of bridging tridentate imine (tpy) coordination on the Cp^*_2Yb ytterbocene electronic structure. This metal−ligand system is appealing since the symmetrical 4′-substituted-tpy provides a route to assembly of multi-metallic constructs possessing axial symmetry along the metal−metal coordinate. This structural aspect is important for identifying nascent structure−property relationships that are dependent on the C_{2v} ligand field of the ytterbocene moiety; binding of Cp^*_2Yb to 4′-substituted-tpy preserves the C_{2v} symmetry of the parent complex while offering a convenient synthetic handle via 4′ substitution.

A number of experimental probes have been brought to bear in an effort to characterize this unusual charge-transfer electronic configuration and to understand its origin. Recently reported electrochemical data reveal a remarkable change in the redox energetics associated with the formation of the base adduct for both the N-heterocyclic ligand-based reduction and the Cp^*_2Yb metal-based oxidation.[1] The ligand LUMO is stabilized as evidenced by a positive shift of nearly 1 V relative to the first reduction potential of the free ligand. The metal-based redox orbital is destabilized (negative potential shift), also by ∼1 V, relative to the reduction potential for the THF adduct, $Cp^*_2Yb(thf)_n$. Bands in the near-IR region ($E_{00} \approx 5000$ cm^{-1}) of the electronic absorption spectra for both bpy and phen adducts were assigned to the optically induced ligand-to-metal ($\pi^* \rightarrow$ f) charge-transfer transition.[1] These are the optical analogue (the converse) of the spontaneous electron-transfer phenomenon and occur at an energy consistent with predictions based on the separation between the ligand-based oxidation and metal-based reduction in the adducts (∼0.8 V).[1]

The magnetic properties of these systems have been investigated by variable temperature magnetic susceptibility. Although the specific details of the magnetic coupling between metal-based and ligand-based spins are not the same for all adducts, some trends have been noted. For example, Andersen and co-workers have observed temperature-dependent magnetic behavior for 1:1 Yb imine adducts and have described this as antiferromagnetic coupling between the Yb^{III} center and the ligand radical anion.[3,4] More recently, we have proposed an alternative description of this behavior for the 1:1 adducts of tpy and tpy-CN using a valence tautomer model. This model attributes the magnetic behavior to a thermally induced equilibrium between the paramagnetic [$(f)^{13}-(\pi^*)^1$] and the diamagnetic [$(f)^{14}-(\pi^*)^0$] form of the complex.[2] For the 2:1 adducts studied thus far, the paramagnetic centers on the two f^{13} metal fragments are reported to couple antiferromagnetically at low temperature through what has been interpreted as a polarization mechanism.[3]

Our intent in this paper is two-fold: (1) to explore the concomitant alterations in electron-density distributions and spatial extents in the LUMO of the N-heterocyclic ligand as compared to monometallic complexes, and (2) to determine the influence of increased metal−metal separation on the mechanism and/or magnitude of the electronic/magnetic coupling. In this work, we present synthetic and structural results together with detailed cyclic voltammetric, UV−vis-near-IR electronic absorption spectral data and magnetic susceptibility measurements of the 2:1 adducts with tetra(2-pyridyl)pyrazine (tppz) (**1**), 6′,6″-bis(2-pyridyl)-2,2′:4′,4″:2″,2‴-quaterpyridine (qtp) (**2**), and 1,4-di(4′-terpyridyl)-benzene (dtb) (**3**) (Chart 1).

Chart 1. Molecular Wire Complexes **1**−**3**

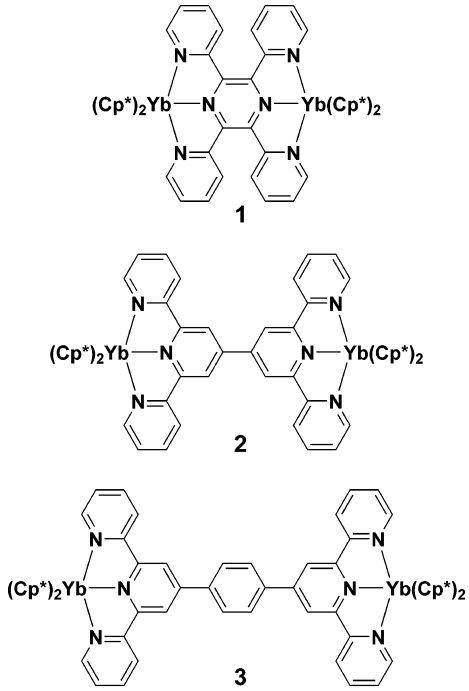

Experimental Section

Syntheses. All reactions and product manipulations were carried out under an atmosphere of dry argon or helium using standard drybox or Schlenk techniques. Anhydrous solvents, tetrahydrofuran (THF), toluene, and methylene chloride were purchased from Aldrich or Acros and stored in the glovebox over activated 4 Å molecular sieves overnight and passed the ketyl test before use. $Cp^*_2Yb{\cdot}OEt_2$,[10] $Cp^*_2Yb(tpy)$ (**4**)[2] and $AgBPh_4$[11] were prepared according to the literature procedures. $AgB(C_6H_3\text{-}(3,5\text{-}CF_3)_2)_4$ was prepared in a manner analogous to $AgBPh_4$ using $NaB(C_6H_3\text{-}(3,5\text{-}CF_3)_2)_4$.[11] $AgPF_6$, $[Cp_2Fe]PF_6$, and the ligands 2,2′:6′,2″-terpyridine (tpy), tetra(2-pyridyl)pyrazine (tppz), and 1,4-di(terpyridyl)-benzene (dtb) were purchased from Aldrich and used as received. The ligand 6′,6″-bis(2-pyridyl)-2,2′:4′,4″:2″,2‴-quaterpyridine (qtp) was purchased from Hetcat and used as received. Na^+-

(8) Coronado, E.; Palacio, F.; Veciana, J. *Angew. Chem., Int. Ed.* **2003**, *42*, 2570.
(9) (a) Inoue, J.; Ohno, H. *Science* **2005**, *309*, 2004 ; Tang, H. X.; Masmanidis, S.; Kawakami, R. K.; Awschalom, D. D.; Roukes, M. L. *Nature* **2004**, *431*, 52. (b) Peplow, M. *Nature* **2005**, *435*, 71.
(10) Tilley, T. D.; Boncella, J. M.; Berg, D. J.; Burns, C. J.; Andersen, R. A. *Inorg. Synth.* **1990**, *27*, 146.
(11) Jordan, R. F.; Echols, S. F. *Inorg. Chem.* **1987**, *26*, 383.

$(tpy)^-$, $K^+(tppz)^-$, $K^+(qtp)^-$ and $K^+(dtb)^-$ were prepared by adding one equivalent of freshly cut alkali metal to one equivalent of tpy, tppz, qtp, and dtb, respectively, in THF and stirring overnight at room temperature. Elemental analyses were performed by Midwest Microlab, Indianapolis, IN. The synthesis of $Cp^*_2Yb(tpy)^+$ ([**4**]$^+$) has been reported previously, but with $Cp^*_2YbI_2^-$ as the counterion.[2]

$(Cp^*_2Yb)_2(tppz)$ (1). A room-temperature toluene solution (15 mL) of $Cp^*_2Yb{\cdot}OEt_2$ (500 mg, 0.97 mmol) was added to solid tppz (188 mg, 0.48 mmol). The solution immediately darkened and was stirred vigorously overnight. The toluene was removed under vacuum, and the resultant dark green powder was taken up in a minimum amount of boiling toluene (approximately 5 mL), filtered hot through a filter paper plug, and the solution allowed to cool to room temperature. The cooled solution was then placed in the glovebox freezer overnight (−35 °C) and the dark crystals that formed were collected by filtration (486 mg 0.39 mmol, 81%). Anal. Calcd for $C_{64}H_{78}N_6Yb_2$: C, 60.27; H, 6.01; N, 6.59. Found: C, 61.85; H, 5.98; N, 6.81. ^{1}H NMR (THF-d_8): δ 51.01 (s, tppz), 15.33 (s, tppz), 14.68 (s, tppz), 9.31 (s, tppz), 1.48 (s, Cp*).

$[(Cp^*_2Yb)_2(tppz)]BPh_4$ ([1]$^+$). A room-temperature THF solution (15 mL) of $(Cp^*_2Yb)_2$(tppz) (50 mg, 0.04 mmol) was added to one equivalent of solid $AgBPh_4$ (17 mg, 0.04 mmol) with stirring overnight. THF was removed under vacuum and the resulting solid was extracted into CH_2Cl_2 (10 mL) and filtered over a filter paper plug. Removal of CH_2Cl_2 yielded a purple, analytically pure powder (53 mg, 0.04 mmol, 95%) that can be recrystallized by diffusion of pentane into a CH_2Cl_2 solution. Anal. Calcd. for $C_{88}H_{96}N_6B_1Yb_2$: C, 66.18; H, 6.06; N, 5.27. Found: C, 66.46; H, 5.99; N, 5.67. ^{1}H NMR (CD_2Cl_2): δ 95.20 (s, tppz), 27.16 (s, tppz), 2.61 (s, Cp*), −10.77 (s, tppz), −36.55 (s, tppz).

$[(Cp^*_2Yb)_2(tppz)][PF_6]_2$ ([1]$^{2+}$). A room-temperature THF solution (15 mL) of $(Cp^*_2Yb)_2$(tppz) (42 mg, 0.03 mmol) was added to two equivalents of solid $AgPF_6$ (17 mg, 0.06 mmol) with stirring overnight. THF was removed under vacuum and the resulting solid was extracted into CH_2Cl_2 and filtered over a filter paper plug. Removal of CH_2Cl_2 yielded a brown, analytically pure powder (49 mg, 0.03 mmol, quantitative yield). Anal. Calcd. for $C_{65}H_{78}N_6P_2F_{12}Yb_2{\cdot}CH_2Cl_2$: C, 47.31; H, 4.76; N, 5.09. Found: C, 47.36; H, 4.79; N, 5.16. ^{1}H NMR (CD_2Cl_2): δ 81.57 (s, tppz), 23.77 (s, tppz), 3.18 (s, Cp*). The other tppz resonances were not observed.

$(Cp^*_2Yb)_2(qtp)$ (2). A room-temperature toluene solution (10 mL) of $Cp^*_2Yb{\cdot}OEt_2$ (150 mg, 0.29 mmol) was added to the solid qtp ligand (66 mg, 0.14 mmol) with stirring overnight. The toluene was removed under vacuum to yield a teal powder (183 mg, 0.135 mmol, 97%). Anal. Calcd. for $C_{70}H_{80}N_6Yb_2$: C, 62.11; H, 5.96; N, 6.21. Found: C, 61.00; H, 6.33; N, 6.07. ^{1}H NMR (THF-d_8, 400 MHz): δ 45.15 (s, qtp), 29.42 (s, qtp), 15.25 (s, qtp), −4.91 (s, Cp*). The other qtp resonances were not observed.

$[(Cp^*_2Yb)_2(qtp)]BPh_4$ ([2]$^+$). Solid $(Cp^*_2Yb)_2$(qtp) (30 mg, 0.02 mmol) and $[(Cp^*_2Yb)_2(qtp)]^{2+}$ (44 mg, 0.02 mmol) were placed in vial equipped with a stirring bar. THF (10 mL) was added to the vial and the solution stirred at room-temperature overnight. The THF was removed under vacuum, and the solid was extracted into CH_2Cl_2 (10 mL) and filtered over a filter paper plug. CH_2Cl_2 was removed under vacuum to yield a dark blue powder, **[2]**$^+$, (62 mg, 0.037 mmol, 93%). Anal. Calcd. for $C_{82}H_{95}N_6BYb_2$: C, 64.74; H, 6.25; N, 5.53. Found: C, 65.04; H, 6.17; N, 5.43. ^{1}H NMR (CD_2Cl_2, 400 MHz): δ 17.24 (s, qtp), 13.26 (s, qtp), 7.12 (m, BPh_4), 7.04 (m, BPh_4), 6.88 (m, BPh_4), −0.64 (s, Cp*). The other qtp resonances were not observed.

$[(Cp^*_2Yb)_2(qtp)][BPh_4]_2$ ([2]$^{2+}$). A room-temperature THF solution (10 mL) of $(Cp^*_2Yb)_2$(qtp) (65 mg, 0.05 mmol) was added to 2 equiv. of solid $AgBPh_4$ (43 mg, 0.10 mmol) in a vial with stirring overnight. THF was removed under vacuum and the solid was extracted into CH_2Cl_2 (10 mL) and filtered over a filter paper plug. CH_2Cl_2 was removed under vacuum to yield a dark purple powder (81 mg, 0.04 mmol, 82% yield). Anal. Calcd. for $C_{118}H_{120}N_6B_2Yb_2{\cdot}3.5CH_2Cl_2$: C, 63.80; H, 5.59; N, 3.67. Found: C, 63.59; H, 5.56; N, 3.13. %). ^{1}H NMR (CD_3CN, 400 MHz): δ 63.17 (qtp), 39.29 (qtp), 29.62 (qtp), 19.72 (qtp), 17.02 (qtp), 7.18 (m, BPh_4), 7.04 (m, BPh_4), 6.87 (m, BPh_4), −0.08 (s, Cp*).

$(Cp^*_2Yb)_2(dtb)$ (3). A room-temperature toluene solution (15 mL) of $Cp^*_2Yb{\cdot}OEt_2$ (205 mg, 0.39 mmol) was added to the solid dtb ligand (106 mg, 0.19 mmol) with stirring. Toluene was removed under vacuum to yield complex **3** (280 mg, 0.19 mmol, quantitative yield). Anal. Calcd. for $C_{76}H_{84}N_6Yb_2$: C, 63.84; H, 5.93; N, 5.88. Found: C, 65.43; H, 5.87; N, 5.79. ^{1}H NMR (THF-d_8, 400 MHz): δ 23.18 (s, dtb), 16.60 (s, dtb), −3.21 (s, Cp*). The other dtb resonances were not observed.

$[(Cp^*_2Yb)_2(dtb)]OTf$ ([3]$^+$). Solid $(Cp^*_2Yb)_2$(dtb) (23 mg, 0.02 mmol) and $[(Cp^*_2Yb)_2(dtb)]^{2+}$ (28 mg, 0.02 mmol) were placed in vial equipped with a stirring bar. THF (10 mL) was added to the vial and the solution stirred at room temperature in the dark overnight. THF was removed under vacuum, and the solid was extracted into CH_2Cl_2 (10 mL) and filtered over a filter paper plug. CH_2Cl_2 was removed to yield complex **[3]**$^+$, (27 mg, 0.02 mmol, 94%). Anal. Calcd. for $C_{77}H_{84}N_6F_3O_4SYb_2(CH_2Cl_2)$: C, 55.84; H, 5.17; N, 5.01 Found: C, 56.09; H, 6.08; N, 4.46. ^{1}H NMR (CD_2Cl_2, 400 MHz): δ 84.48 (s, dtb), 25.20 (s, dtb), 20.28 (s, dtb), 18.46 (s, dtb), −1.36 (s, Cp*).

$[(Cp^*_2Yb)_2(dtb)][OTf]_2$ ([3]$^{2+}$). A room-temperature THF solution (15 mL) of $(Cp^*_2Yb)_2$(dtb) (103 mg, 0.07 mmol) was added to 2 equiv. of solid AgOTf (37 mg, 0.14 mmol) with stirring overnight. THF was removed under vacuum, and the solid was extracted into CH_2Cl_2 (10 mL) and filtered over a filter paper plug. CH_2Cl_2 was removed under vacuum to yield **[3]**$^{2+}$. (112 mg, 0.06 mmol, 97%). ^{1}H NMR (CD_2Cl_2, 400 MHz) δ 74.67 (s, dtb), 31.13 (s, dtb), 29.15 (s, dtb), 22.41 (s, dtb), 20.62 (s, dtb), 19.27 (s, dtb), −1.40 (s, Cp*). Anal. Calcd. for $C_{140}H_{108}N_6B_2F_{48}Yb_2$: C, 53.31; H, 3.45; N, 2.66. Found: C, 52.97; H, 3.72; N, 2.62.

$[Cp^*_2Yb(tpy)]OTf$ ([4]$^+$). A room-temperature THF solution (15 mL) of $Cp^*_2Yb(tpy)$ (100 mg, 0.15 mmol) was added to one equivalent of AgOTf (38, mg, 0.15 mmol). The suspension was stirred vigorously overnight in the dark. THF was removed under vacuum and the residual solid was washed with toluene until the washings were colorless. The remaining solid was then extracted with CH_2Cl_2 (10 mL) and filtered. CH_2Cl_2 removal left the crude product behind as an orange powder. The product was purified by recrystallization by diffusion of pentane into a concentrated CH_2Cl_2 solution of the product. Yield: 71%. ^{1}H NMR (CD_2Cl_2): δ 70.09 (s, tpy), 28.44 (s, tpy), 25.66 (s, tpy), 20.99 (s, tpy), 20.34 (s, tpy), 16.42 (s, tpy), −2.12 (s, Cp*).

X-ray Diffraction. The data for crystals of [**1**]$^+$ and [**4**]$^+$ were collected on a Bruker P4/CCD diffractometer cooled to 203 K using a Bruker LT-2 temperature device. The instrument was equipped with a sealed, graphite monochromatized MoKα X-ray source (λ = 0.71073 Å). A hemisphere of data was collected using φ scans, with 30 s frame exposures and 0.3° frame widths. Data collection and initial indexing and cell refinement were handled using SMART[12] software. Frame integration, including Lorentz-polarization corrections, and final cell parameter calculations were carried out using SAINT[13] software. The data were corrected for absorption using the SADABS[14] program. Decay of reflection intensity was monitored via analysis of redundant frames. The structures were solved using Direct methods and difference Fourier techniques. Attempts to model the disorder in the Cp* ligands in both structures were problematic, and in the final refinement these were modeled as single occupancy sites with large temperature factors. In the structure of [**1**]$^+$ three lattice methylene chloride molecules were refined at reduced occupancies, with C−Cl distances restrained to 1.75(3) Å. The refinement of temperature factors for atoms C(3), C(5), C(9), C(20′), and C(23′) were unstable, and were subsequently restrained. The final refinement included anisotropic temperature factors on all non-hydrogen atoms. Hydrogen atom positions were idealized, and refined using a riding model. Structure solution, refinement, graphics, and creation of publication materials were performed using

(12) *SMART* **1996**, Bruker AXS: Madison, WI 53719.
(13) *SAINT* **1998**, Bruker AXS, Inc.: Madison, WI 53719.
(14) Sheldrick G. M. *SADABS* **1996**, University of Göttingen: Germany.

Table 1. Crystal Data and Data Collection and Refinement Parameters $[1]^+$ and $[4]^+$

	$(Cp^*_2Yb)_2(tppz)^+$	$Cp^*_2Yb(tpy)^+$
empirical formula	$C_{91}H_{102}N_6Cl_6BYb_2$	$C_{36}H_{41}F_3N_3O_3SYb$
Fw	1849.38	825.82
space group	*C*2/*c*	$P2_1$
A, Å	35.22(1)	11.360(3)
B, Å	14.702(5)	15.544(3)
C, Å	37.94(1)	19.137(4)
α, deg	90	90
β, deg	114.365(5)	93.107(4)
γ, deg	90	90
V, Å^3	17896(9)	3374.1(13)
ρ_{calcd}, g cm^{-3}	1.373	1.626
μ, mm^{-1}	2.302	2.891
λ(Mo Kα), Å	0.71073	0.71073
T, K	203	203
GooF[a]	2.507	1.148
*R*1 [$I > 2\sigma(I)$], %[b]	7.92	6.48
w*R*2[$I > 2\sigma(I)$], %[c]	18.08	12.14
*R*1 (all data), %[b]	9.13	7.44
w*R*2 (all data), %[c]	18.36	12.56
largest diff peak/hole, e Å^{-3}	2.736 and −1.992	2.367 and −2.248

[a] GooF = $[\Sigma[w(F_o^2 - F_c^2)]^2/(n-p)]^{1/2}$; n = number of reflections, p = total number of parameters refined. [b] $R1 = \Sigma||F_o| - |F_c||\Sigma|F_o|$. [c] $wR2 = [\Sigma[w(F_o^2 - F_c^2)]^2]/\Sigma[w(F_o^2)^2]]^{1/2}$.

SHELXTL.[15] Additional details of data collection and structure refinement are listed in Table 1.

Magnetic Susceptibility. Magnetic measurements over the temperature range 2 to 350 K were made using a Quantum Design Superconducting Quantum Interference Device (SQUID) magnetometer. The microcrystalline samples were sealed in borosilicate NMR tubes along with a small amount of quartz wool, which held the sample near the tube center. Contributions to the magnetization from quartz wool and tube were measured independently and subtracted from the total measured signal. The magnetic susceptibility, defined as the sample magnetization M divided by the applied magnetic field H, was measured as a function of temperature at an applied field of 0.1 T. Diamagnetic corrections were made using Pascal's constants.

Electrochemistry. Cyclic voltammetric studies were conducted in an inert atmosphere glovebox (nitrogen or helium) using a Perkin-Elmer Princeton Applied Research Corporation (PARC) Model 263 potentiostat under computer control using M270 software. The electrochemical cell was either a modified PARC microcell consisting of a ∼3 mm platinum disk working electrode, a Pt wire counter electrode, and a silver wire quasi-reference electrode or a modified BAS microcell consisting of ∼1.5 mm Pt and Ag disk working and quasi-reference electrodes and a Pt wire counter electrode. All experiments were conducted in purified THF using ∼0.1 M $[(n\text{-}C_4H_9)_4N][B(C_6F_5)_4]$ as the supporting electrolyte. The benefits of this electrolyte for reducing uncompensated resistance in low dielectric solvents such as THF have been previously described.[16] Measured potentials were calibrated using the ferrocene/ferrocenium couple. Data were analyzed using the IGOR Pro (Wavemetrics, Inc.) software package on a Macintosh platform.

Electronic Absorption Spectroscopy. Electronic absorption spectra from ∼200−2200 nm were recorded at room temperature using a Perkin-Elmer Lambda 19 spectrophotometer. Spectra were obtained in anhydrous THF (neutrals) and anhydrous CH_2Cl_2 (cations) against a solvent blank. Quartz cells with 1 cm path-length were used in the UV−visible region. However, for most NIR data, 1 mm path-length quartz cells were used to minimize contributions from solvent absorption band profiles. Typical slit widths were 2 nm in the UV−visible and 5−10 nm in the NIR.

(15) *SHELXTL* **2001**, Bruker AXS: Madison, WI 53719.
(16) (a) LeSuer, R. J.; Geiger, W. E. *Angew. Chem., Int. Ed.* **2000**, *39*, 248. (b) Camire, N.; Mueller-Westerhoff, U. T.; Geiger, W. E. *J. Organomet. Chem.* **2001**, *637*−*639*, 823.

Results and Discussion

Syntheses and Structure. The neutral complexes **1**−**4** (Chart 1 for **1**−**3**) were prepared by adding a toluene solution of $Cp^*_2Yb{\cdot}OEt_2$ to the nitrogen bases. The solubility of these complexes decreases significantly as the molecular weight increases (**4** > **1** > **2** > **3**). The solubility of **4** is sufficient to afford purification from highly concentrated solutions by recrystallization from boiling toluene. Complexes **1**, **2** and **3** are considerably less soluble. However, they can be obtained as analytically pure powders. The dark color of the complexes supports a reduced ligand electronic structure consistent with their ^{1}H NMR spectra, which indicates that they are paramagnetic. The oxidation reactions of the neutral complexes were carried out in a straightforward manner employing common oxidants such as ferrocenium hexafluorophosphate, or various silver salts (AgX; X = I, OTf, PF_6, BPh_4, $B(Ar_F)_4$). It was necessary to draw on the different characteristics of the various counteranions to obtain crystals suitable for X-ray structural analysis.

The structure of **[4]**$^+$ is shown in the Supporting Information. Comparison of the bond distances and bond angles (Table 2) reveals that the mean Yb−N bond distance (2.44 Å) is slightly elongated relative to the neutral congener (2.41 Å). Furthermore, we observe that the Yb−$Cp^*_{centroid}$ bond distance of the tpy cation (2.38 Å) contracts relative to the neutral parent (2.44 Å). These trends are consistent with values observed previously for the bpy complex (Table 2) and can be attributed to electrostatic differences between the two redox congeners.[4] All other coordinates (Table 2) appear to be statistically indistinct between the neutral and cationic forms of the complex with no discernible changes in ligand-based torsion angles.

The monocationic bimetallic **[1]**$^+$ was prepared by oxidation of the previously reported redox congener (**1**) with one equivalent of $AgBPh_4$ (Figure 1). Like **[4]**$^+$, a slight elongation of the Yb−N bond distances and a contraction of the Yb−$Cp^*_{centroid}$ distance are observed upon oxidation of **1** to **[1]**$^+$ (Table 2). The relatively small changes observed in the aforementioned coordinates for the tppz complexes could in part be due to the fact that the charge can now be distributed between two metal sites. A significant lengthening of the Yb−Yb distance is observed upon oxidation (7.57 Å for **1** and 7.628 Å for **[1]**$^+$),[5] which compares to values between 6.2 and 6.9 Å reported for transition-metal, η^3-bound, tppz complexes.[17] In addition to the lengthening of the Yb−Yb distance, a relaxation of the ligand torsion angles ($C_{pyr}-C_{pyz}-C_{pyz}-C_{pyr}$ = 55° for **1** and 39° for **[1]**$^+$) is observed and is evidence that steric repulsion between the two metal centers is significant.[5]

Of the reported bimetallic structures containing the qtp ligand, the average torsion angle between the two tpy portions is

(17) (a) Carranza, J.; Brennan, C.; Sletten, J.; Clemente-Juan, J. M.; Lloret, F.; Julve, M. *Inorg. Chem.* **2003**, *42*, 8716. (b) Sakai, K.; Kurashima, M. *Acta Crystallogr.* **2003**, *E59*, m411. (c) Chanda, N.; Laye, R. H.; Chakraborty, S.; Paul, R. L.; Jeffery, J. C.; Ward, M. D.; Lahiri, G. K. *J. Chem. Soc, Dalton Trans.* **2002**, 3496. (d) Campos-Fernández, C. S.; Smucker, B. W.; Clérac, R.; Dunbar, K. R. *Isr. J. Chem.* **2001**, *41*, 207. (e) Yamada, Y.; Miyashita, Y.; Fujisawa, K.; Okamoto, K. *Bull. Chem. Soc. Jpn.* **2000**, *73*, 1843. (f) Teles, W.; Speziali, N. L.; Filgueras, C. A. L. *Polyhedron* **2000**, *19*, 739. (g) Hagrman, D.; Hagrman, P.; Zubieta, J. *Inorg. Chim. Acta* **2000**, *300*−*302*, 212. (h) Hartshorn, C. M.; Daire, N.; Tondreau, V.; Loeb, B.; Meyer, T. J.; White, P. S. *Inorg. Chem.* **1999**, *38*, 3200. (i) Koman, M.; Balaghova, Z.; Valigura, D. *Acta Crystallogr., C* **1998**, *54*, 1277. (j) Graf, M.; Greaves, B.; Stoeckli-Evans, H. *Inorg. Chim. Acta* **1993**, *204*, 239. (k) Graf, M.; Stoeckli-Evans, H.; Escuer, A.; Vicente, R. *Inorg. Chim. Acta* **1997**, *257*, 89.

Table 2. Selected Bond Distances (Å) and Angles (deg) for Ytterbocene Complexes[a]

	$Cp^*_2Yb(bpy)$[b]	$Cp^*_2Yb(bpy)^{+}$[b]	4[c]	$[4]^+$	1[c]	$[1]^+$
			bond lengths			
$Yb-N_{mean}$	2.32	2.37	2.41	2.44	2.43	2.45
$Yb-N_{central}$	NA	NA	2.41(1)	2.440[9]	2.42[1]	2.438[9]
$Yb-N_{terminal}$	NA	NA	2.42(1)	2.433[9]	2.43[1]	2.452[9]
Yb−Yb	NA	NA	NA	NA	7.57	7.628
$Yb-Cp^*_{cent}$	2.34	2.30	2.44	2.38	2.42	2.406
			bond angles			
Cp^*_{cent}-Yb−Cp^*_{cent}	139.3	141.5	138.3	139.3	140	139.2
$Cp^*_{cent}-Yb(1)-Yb(2)-Cp^*_{cent}$	NA	NA	NA	NA	35	32
C_{pyr}-C_{pyz}-C_{pyz}-C_{pyr}	NA	NA	NA	NA	55	39
N_{pyr}-C_{pyr}-C_{pyz}-N_{pyz}	3	7	1	3	24	18

[a] Esd's (standard deviations) are given in parentheses. Values in square brackets are arithmetic means of esd's. [b] Data taken from ref 4. [c] Data taken from ref 5.

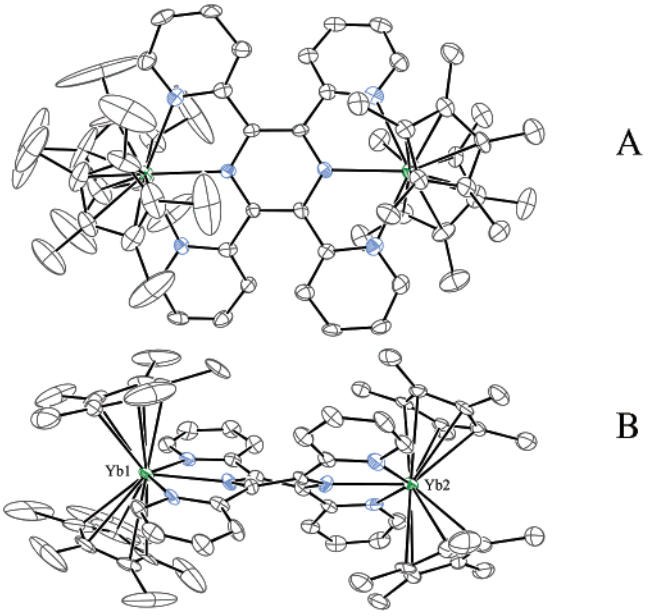

Figure 1. Thermal ellipsoid representation of **[1]**$^+$ (35% probability ellipsoids). (A) Top view. (B) Side view. The BF_4^- anion, solvent, and hydrogen atoms have been omitted for clarity.

approximately 4° and metal−metal separations range from 10.8 to 11.5 Å.[18,19] For the two reported bimetallic dtb structures, one has a torsion angle (defined by the angle between the bridging aryl group and the tpy portion of the ligand) of 3.6°, whereas the other possesses an angle of 37.6°; the angle between the two tpy fragments are 6.1 and 2.3° respectively with corresponding metal−metal separations of 15.2 and 15.7 Å.[19,20] Our expectation for the qtp and dtb structures discussed within this manuscript is that the bridging ligands will be nearly planar in the solid state. This is borne out by the fact that the structure of the related qtp complex, $[(C_5Me_4Et)_2Yb]_2$qtp, possesses a tpy-tpy torsion angle of 0.4° and a metal separation of 11.8 Å (see Supporting Information). Furthermore, the electronic behavior of these complexes (see below) suggests that there is significant electronic interaction across the bridging ligand, which precludes an orthogonal orientation of the two Cp^*_2Yb-(tpy) fragments.

(18) (a) Ouellette, W.; Golub, V.; O'Connor, C. J.; Zubieta, J. *Dalton Trans.* **2005**, 291. (b) Koo, B.-K.; Ouellette, W.; Burkholder, E. M.; Golub, V.; O'Connor, C. J.; Zubieta, J. *Solid State Sci.* **2004**, *6*, 461.
(19) Koo, B.-K.; Bewley, L.; Golub, V.; Rarig, R. S.; Burkholder, E.; O'Connor, C. J.; Zubieta, J. *Inorg. Chim. Acta* **2003**, *351*, 167.
(20) Maekawa, M.; Minematsu, T.; Konaka, H.; Sugimoto, K.; Kuroda-Sowa, T.; Suenaga, Y.; Munakata, M. *Inorg. Chim. Acta* **2004**, *357*, 3456.

Magnetic Susceptibility. The magnetic susceptibilities (χ) for compounds **1**, **2** and **3** were measured as a function of temperature and are presented in Figures 2A−C, respectively. The temperature dependence observed for the χ^{-1} vs T plots reveal that the **1** and **3** complexes obey the Curie−Weiss law to approximately 50 K, below which, the χ^{-1} vs T data begins to diverge from linearity. This departure from the Curie−Weiss law could be due to the presence of trace Yb^{III} impurities; however, this is unlikely since the observed χ^{-1} vs T divergence is present for multiple samples prepared from different syntheses for all of the neutral complexes under investigation. For the qtp species, the χ vs T data increase and achieve a maximum at approximately 13 K. This feature is reproducible for multiple samples prepared from different formulations and is indicative of Yb^{III}-Yb^{III} antiferromagnetic spin exchange mediated by the bridging ligand.

The interpretation of the magnetic data is based on the fact that the neutral, monocationic and dicationic configurations are $[(f)^{13}-(\pi^*)^2-(f)^{13}]$, $[(f)^{13}-(\pi^*)^1-(f)^{13}]$, and $[(f)^{13}-(\pi^*)^0-(f)^{13}]$ respectively. This is borne out by the fact that the room-temperature moments (μ_{eff}) are 6.33, 5.42, and 5.70 μ_B for complexes **1**, **2**, and **3**, respectively. For two noninteracting Yb^{III} centers bridged by a diamagnetic ligand, the predicted Curie-Law value for two uncoupled Yb^{III} ions is 6.4 μB in the temperature region of 90 K and above.[3]

As a framework for this discussion, we will make use of the three classes described by Andersen and co-workers for a related set of 2:1 metal-to-ligand neutral adducts $(Cp^*_2Yb)_2(\mu$-L) (L = 2,2′-bipyrimidine, 2,2′-azopyridine, 2,3-di-(2′-pyridino)quinoxaline).[3] Only Class 2 and 3 behaviors apply to the materials presented in this study since Class 1 complexes include 1:1 and 1:2 metal-to-ligand adducts only. Class 2 and 3 materials are 2:1 adducts in which the Yb(III) fragments are joined by a dianionic/diamagnetic bridging ligand. However, the bridging ligand does not facilitate magnetic exchange between the two Yb(III) centers for Class 2 complexes, whereas Class 3 materials exhibit an antiferromagnetic exchange coupling at low temperatures. The magnetic coupling observed for materials such as $(Cp^*_2Yb)_2(\mu$-bipyrimidine) has been explained using an electrostatic polarization mechanism in which the dianionic/diamagnetic ligand bridge L($\alpha\beta$) invokes spin correlation of the type Yb(α)L($\alpha\beta$)Yb(β). Correlation of the metal and ligand spins is postulated to occur via an electrostatic interaction rather than a through-orbital/superexchange mechanism.

Complex **1** displays magnetic behavior associated with the Class 2 description as no significant change in χ^{-1} vs T is

Table 3. Summary and Comparison of Redox Data[a] for Ytterbocene Complexes and Ruthenium(II) Congeners

	ligand-based		metal-based		
	$E_{1/2}(L_1)$	$E_{1/2}(L_2)$	$E_{1/2}(M_a)$	$E_{1/2}(M_b)$	$\lvert\Delta(E_{1/2})[M-L]\rvert$[b]
tpy	−2.66				
4	−1.72		−2.56		0.84
tppz	−2.18	−2.61			
1	−0.58	−1.41	−2.21	−2.81	0.80
qtp	−2.22	−2.80			
2	−1.12	−1.61	−2.57	−2.79	0.96
dtb	−2.32	−2.54			
3	−1.45	−1.64	−2.37	−2.59	0.73

							[(ttpy)Ru(BL)Ru(ttpy)]$^{4+}$[c]		
	tppz	**1**	qtp	**2**	dtb	**3**	tppz	qtp	dtb
$\lvert\Delta(E_{1/2})[M_a\text{-}M_b]\rvert$	-	0.60	-	0.22	-	0.22	0.30(0.31)[d]	0	0
$\lvert\Delta(E_{1/2})[L_1\text{-}L_2]\rvert$	0.43	0.83	0.58	0.49	0.22	0.19	0.50(0.47)[d]	0.31	0

[a] All values in volts. $E_{1/2}$ values are versus $[(C_5H_5)_2Fe]^{+/0}$ in 0.1 M $[(n\text{-}C_4H_9)_4N][B(C_6F_5)_4]$/THF at room temperature. [b] Separation in $E_{1/2}$ values between most positive metal-based reduction wave and most negative ligand-based oxidation wave. [c] Data from ref 25b except where noted. ttpy = 4′-tolyl-2,2′:6′,2″-terpyridine. BL = bridging ligand as noted. Data collected in 0.1 M $[(n\text{-}C_4H_9)_4N]BF_4/CH_3CN$ at room temperature. [d] Data for $[(tpy)Ru(tppz)Ru(tpy)]^{4+}$ in 0.1 M $[(n\text{-}C_4H_9)_4N]ClO_4/CH_3CN$ at room temperature from ref 25a.

observed at lower temperatures. Complex **2**, on the other hand, displays a prominent feature in χ vs. T, achieving a maximum at 13 K. The observed behavior of **2** is consistent with Class 3 behavior. The χ^{-1} vs T plot for **3** displays a feature at approximately 10 K that may be due to an antiferromagnetic coupling effect, but it is masked by the Curie tail making it difficult to definitively assign Class 2 or Class 3 behavior to this complex. The presence of intermolecular magnetic coupling in these systems is excluded based on their crystal structures. The **1** and $[\mathbf{1}]^+$ complexes possess intermolecular imine-centroid separations that are greater than 6.5 and 7.7 Å respectively.[5] In addition, the related qtp complex $[(C_5Me_4Et)_2Yb]_2$qtp displays intermolecular imine-centroid separations that are greater than 5.6 Å (see Supporting Information).

One of the proposed requirements for the Class 3 materials is that the second reduction potential for the free ligand be more negative than ∼−2.0 V (vs SCE in CH_3CN) so that the energy of the ligand LUMO is properly poised to facilitate metal−metal electronic interaction.[3] In addition, Class 3-membership requires that the singlet configuration associated with the diamagnetic ligand dianion be sufficiently polarizable to induce metal−metal magnetic coupling. Complexes **1**, **2** and **3** satisfy the first requirement (Table 3),[21] but **1** apparently fails to fulfill the polarization requirement necessary for spin correlation. In an attempt to better understand the nature of the ligand dianion polarizability, we have performed a theoretical analysis of the ligand-based LUMOs using Hartree−Fock methods (Supporting Information). The LUMO of the ligand in complex **2** bears a significant resemblance to the LUMO of bipyrimidine[3] in that it possesses the same nodal pattern distributed over the same number of atoms. The LUMOs associated with the ligands of **1** and **3**, on the other hand, are relatively diffuse. We propose that the diffuse nature of the ligand-based LUMOs for **1** and **3**, (coupled with the large Yb−Yb separation in **3**), impairs the ability of the electrons in these orbitals to polarize the Yb(III) spins, whereas the more compact LUMO associated with the ligand of **2** is sufficiently polarizable to facilitate antiferromagnetic exchange.

On the basis of previous investigations of the magnetic-susceptibility behavior of Cp^*_2YbL (L = bpy, tpy, tpy-CN) complexes, it is anticipated that the bimetallic complexes might display the valence tautomeric behavior exhibited by the monometallic analogues.[2,4] The valence tautomer model for the monometallic systems is based upon an equilibrium that exists between the diamagnetic $[(f)^{14}-(\pi^*)^0]$ and paramagnetic $[(f)^{13}-(\pi^*)^1]$ forms of Cp^*_2YbL. We estimate the $\%(f^{13})$ contribution to this equilibrium by comparing the χT values for the neutral monometallics to their cationic congeners in which the configuration is solely $[(f)^{13}-(\pi^*)^0]$. A correction of 0.375 emu K mol^{-1} was made to the neutral species to account for the ligand radical spin. The ratio of the corrected χT value for the neutral complex divided by the pure f^{13} monocation χT value provided room-temperature f^{13} percentages of 28% and 69% for Cp^*_2-Yb(bpy) and Cp^*_2Yb(tpy), respectively. In the case of the bimetallic species, the bridging ligand dianion is diamagnetic and no correction is necessary to account for the ligand spins. Comparison of the neutral/dicationic χT ratios provides room-temperature f^{13} percentages of 95%, 99%, and 93% for **1**, **2** and **3** respectively. The metal-to-ligand electron transfer is essentially complete in these neutral bimetallic species, and there should be no expectation of a temperature-dependent valence tautomer effect for the 2:1 adducts. Furthermore, χT vs T plots of the neutral congeners do not display the sigmoidal profile associated with valence tautomerism (Supporting Information).[22] We believe the absence of valence tautomerism for these bimetallic complexes is due in large measure to the stability of the spin-paired electron configuration on the bridging ligand.

Electrochemistry. Room-temperature cyclic voltammograms for the free ligands, the ytterbocene precursor $Cp^*_2Yb(THF)_n$, and neutral complexes **1**−**4** in 0.1 M $[(n\text{-}C_4H_9)_4N][B(C_6F_5)_4]$/THF are presented in Figure 3. Metrical data extracted from these cyclic voltammograms are summarized in Table 3. The data for **1** and **4** and their corresponding polypyridyl ligands have been reported by us previously,[2,5] but are reproduced here

(21) An approximate comparison of redox potentials in CH_3CN vs SCE to those in THF vs.$[(C_5H_5)_2Fe]^{+/0}$ is obtained by adding 0.4 V to the values in Table 3.

(22) (a) Schultz, D. A. *Magnetism: Molecules to Materials II: Molecule-Based Materials*; Wiley-VCH: Weinheim, Germany, 2002. (b) Hendrickson, D. N.; Pierpont, C. G. *Topics in Current Chemistry*; Springer-Verlag: Berlin, 2004. (c) Pierpont, C. G. *Coord. Chem. Rev.* **2001**, *219*−*221*, 415.

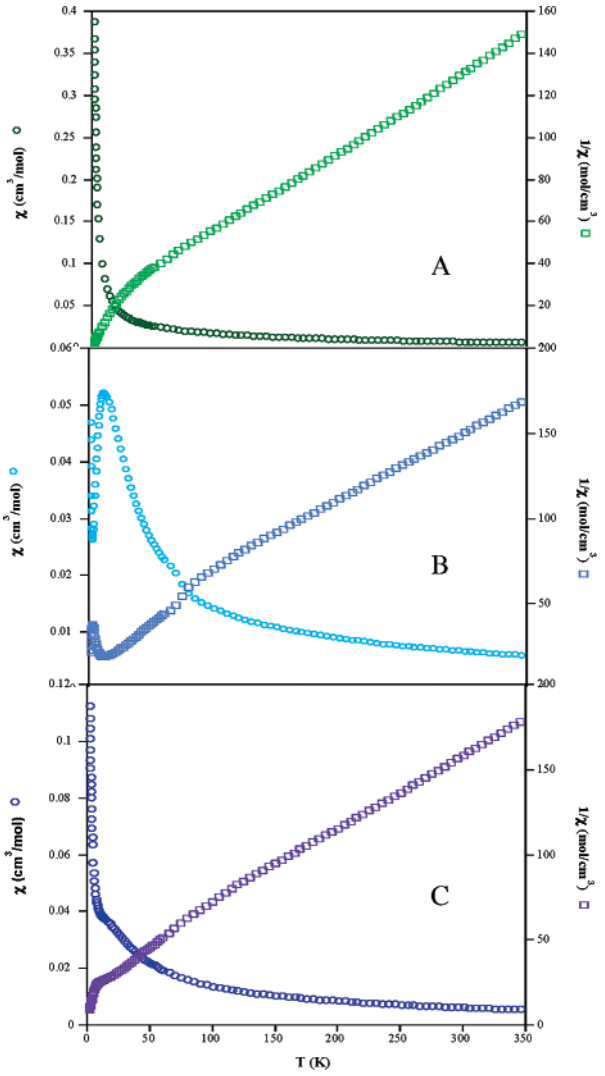

Figure 2. χ (○) and $1/\chi$ (□) vs T for $(Cp^*_2Yb)_2BL$ at 0.1 T. (A) BL = tppz, (B) BL = qtp, (C) BL = dtb.

for comparison. The free ligands qtp and dtb exhibit very low solubility in all common electrochemical solvents, so background charging currents were comparable in magnitude to the Faradaic current of the analytes for these two samples. Note that all bridging terpyridyl-based ligands exhibit two or more reversible reduction waves within the available potential window of this solvent/supporting electrolyte system, although the second reduction step for qtp is only reversible at fast scan rates. These reduction processes in the free ligands are assigned to two successive one-electron additions to the lowest unoccupied molecular orbital (LUMO) to give $(\pi^*)^1$ and $(\pi^*)^2$ electronic configurations, respectively. Thus, the potential separation between the two waves for the ligands ($\Delta(E_{1/2})[L_1 - L_2]$ in Table 3) is a rough measure of the spin-pairing energy for the two electrons in the LUMO.[23] The reversible oxidation wave for the ytterbocene thf adduct is attributed to the one-electron oxidation of the ytterbium metal center, $4f^{14} \rightarrow 4f^{13}$ as noted previously.[1,2,5]

For each of the bimetallic complexes, **1**−**3**, there are two reduction waves and two oxidation waves observed in the potential region from ∼0 to − 3.0 V vs $[Cp_2Fe]^{+/0}$ (Figure 3).

(23) Vlcek, A. A. *Coord. Chem. Rev.* **1982**, *43*, 39.

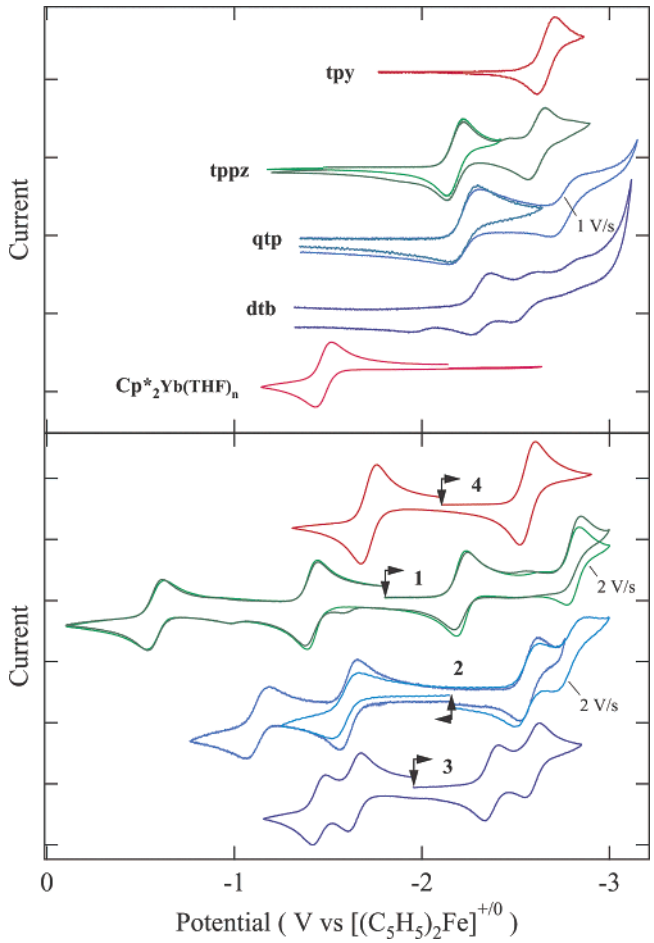

Figure 3. Cyclic voltammograms at a Pt disk working electrode in 0.1 M $[(n\text{-}C_4H_9)_4N][B(C_6F_5)_4]$/THF at room temperature. Scan rates were 200 mV/s unless otherwise indicated. Concentrations of all analytes were ∼5 mM. Currents are in arbitrary units to facilitate comparisons. The vertical arrows indicate the rest potential for each system, and the horizontal arrows indicate the initial scan direction.

Additional irreversible voltammetric waves are also seen at ∼+1 V and more negative than − 3 V vs $[Cp_2Fe]^{+/0}$. The former are attributed to oxidation of the Cp* ligands as noted previously,[1,2,5] and the latter are believed to be further polypyridyl ligand-based reductions. The four waves shown for **1**−**3** are all chemically reversible one-electron processes at all scan rates with the exception of the second reduction wave for **1** and **2** that becomes reversible only at fast scan rates. All four redox processes appear to exhibit slight deviations from Nernstian behavior ($\Delta E_p \approx 60$ mV), but no attempt was made to probe the heterogeneous electron-transfer kinetics in detail.

The remarkable change in the redox energetics for many of these ytterbocene complexes upon formation of adducts of polypyridyl ligands has been described previously.[1,2,5] For **4**, all physical characterization data (magnetic susceptibility, NMR, optical) attest to the dominance of the paramagnetic $[(f)^{13}\text{-}(\pi^*)^1]$ Yb(III)$tpy^{\bullet-}$ species at room temperature in the solid state and in solution. Thus, the voltammetric waves must be ascribed to a metal-based one-electron reduction step ($4f^{13} \rightarrow 4f^{14}$) and a ligand-based one-electron oxidation step ($tpy^{\bullet-} \rightarrow tpy^0$).[2] A similar suite of characterization data for the bimetallics systems **1**−**3** is presented here that also attests to the dominance of paramagnetic species at room temperature. These data, as well as those presented previously by Andersen and co-workers for

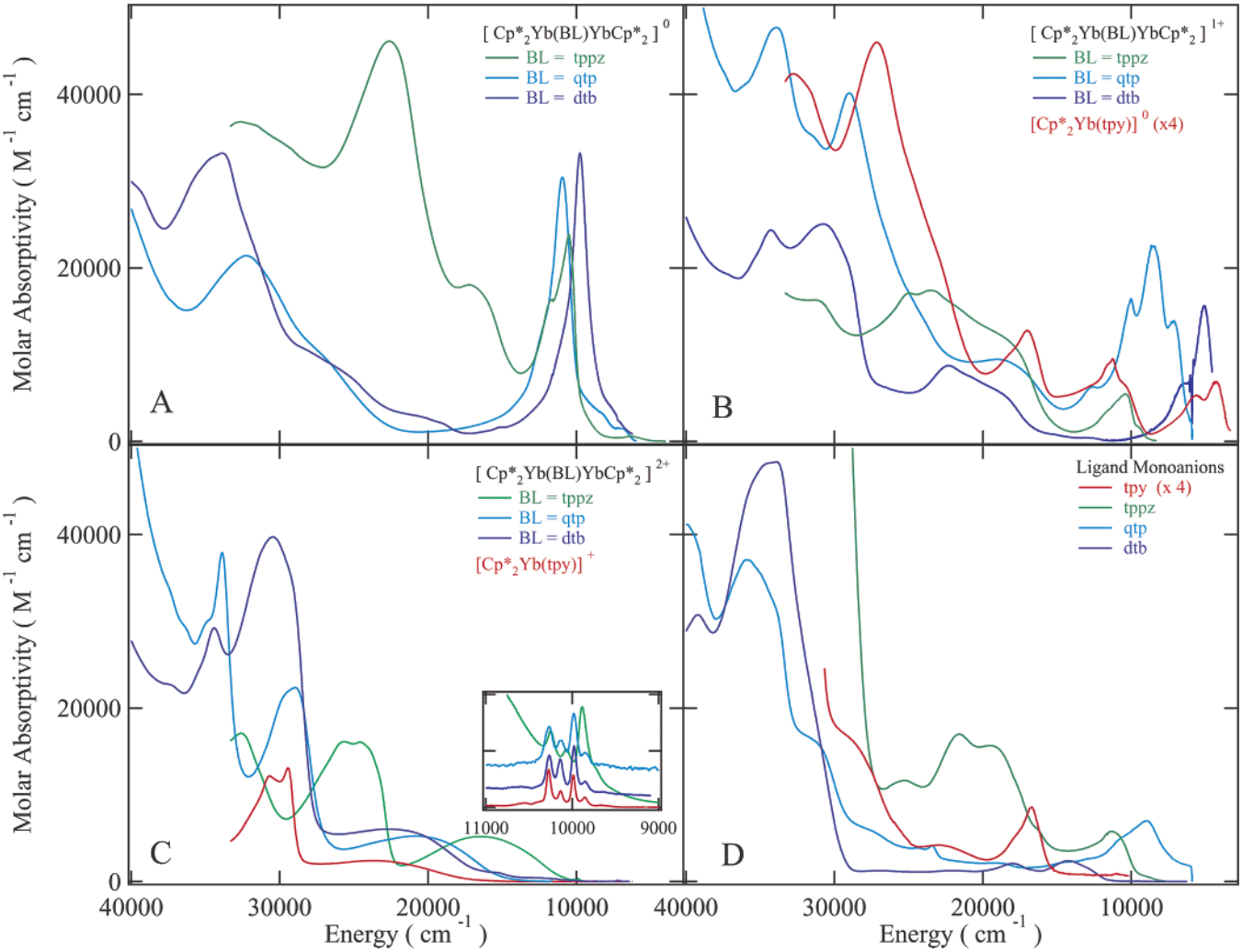

Figure 4. UV−vis−near-IR electronic absorption spectra in CH_2Cl_2 (salts) or THF (neutrals) at 300 K for (A) $[(Cp^*_2Yb(BL)YbCp^*_2]^0$; (B) $[(Cp^*_2Yb(BL)YbCp^*_2]^+$; (C) $[(Cp^*_2Yb(BL)YbCp^*_2]^{2+}$; (D) Ligand Monoanions.

other N-heterocylic ligand-bridged ytterbocene bimetallic complexes,[3] are all consistent with a description of the electronic configuration for the neutral bimetallic complexes as $[(f)^{13}-(\pi^*)^2-(f)^{13}]$ (i.e.,Yb(III)-BL^{2-}-Yb(III); BL = tppz, qtp, and dtb). Therefore, by analogy to the data for **4** and other monometallic ytterbocene polypyridyl adducts, the voltammetric waves for **1**−**3** in Figure 4 can be ascribed to two successive one-electron oxidations of the bridging ligand and a one-electron reduction of each of the two ytterbium metal centers.

One of the most important diagnostic aspects of these voltammetric data is the potential separation between waves, as this metric provides direct information on the degree of electronic interaction between the metal centers and between each metal center and the bridging ligand. These data are summarized in Table 3. The most salient parameter to assess the electronic interactions is the potential separation between the waves associated with the metal-based processes ($\Delta(E_{1/2})$-$[M_a-M_b]$ in Table 3). While this metric has been shown recently to be sensitive to ion-pairing and solvation effects, and can be varied significantly by changing the solvent/supporting electrolyte composition,[24] we have deliberately kept the solvent/supporting electrolyte system (THF/∼0.1 M $[(n\text{-}C_4H_9)_4N]$-$[B(C_6F_5)_4]$) constant throughout the studies reported here. Thus, comparisons of $\Delta(E_{1/2})$ values among these ytterbocene complexes remain strictly valid and informative of *differences* in the extent of electronic communication in a relative sense among these three systems. We have also included published data for the structurally related bimetallic ruthenium complexes of these same bridging ligands ($[(ttpy)Ru(BL)Ru(ttpy)]^{4+}$ and $[(tpy)Ru(BL)Ru(tpy)]^{4+}$; BL = tppz, qtp, dtb; ttpy = 4′-tolyl-2,2′:6′,2″-terpyridine)[25] to provide some basis for comparison of metal−metal interactions across nearly identical bridging-ligand distances.

In the absence of any metal−metal interaction, one might expect the metal-based processes to occur at the same potential (i.e., two superimposed one-electron waves) with perhaps a slight offset (∼ 36 mV) due to statistical (entropic) factors.[26] The actual value is quite large for **1** (600 mV) for which the metal−metal distance is smallest (7.57 Å), but remains significant even for the bridging-ligand complexes having larger metal−metal separation (220 mV for both **2** and **3**). Notably,

(24) (a) Yeomans, B. D.; Kelso, L. S.; Tregloan, P. A.; Keene, F. R. *Eur. J. Inorg. Chem.* **2001**, 239−246. (b) Barriere, F.; Camire, N.; Geiger, W. E.; Mueller-Westerhoff, U. T.; Sanders, R. *J. Am. Chem. Soc.* **2002**, *124*, 7262−7263. (c) D'Alessandro, D. M.; Keene, F. R. *Dalton Trans.* **2004**, 3950−3954. (d) Barriere, F.; Geiger, W. E. *J. Am. Chem. Soc.* **2006**, *128*, 3980−3989.

(25) a) Arana, C. R.; Abruna, H. D. *Inorg. Chem.* **1993**, *32* 194. (b) Collin, J.-P.; Laine, P.; Launay, J.-P.; Sauvage, J.-P.; Sour, A. *J. Chem. Soc., Chem. Commun.* **1993**, 434.

(26) Bard, A. J.; Faulkner, L. R. *Electrochemical Methods: Fundamentals and Applications*; John Wiley and Sons: New York, 2001.

for the corresponding bimetallic ruthenium complexes (for which the voltammetric waves are oxidative in nature), the separation is ~300 mV for the tppz system, but goes to zero for both qtp and dtb. A key difference between the ytterbocene systems and the corresponding bimetallic ruthenium complexes is the electronic configuration on the bridging ligand. For the ytterbocene complexes, the metal-based reduction waves occur in the presence of a doubly reduced bridging ligand. For the ruthenium complexes, the metal-based oxidation waves occur with a neutral ligand connecting the metal centers. Apparently, electron occupation in the antibonding ligand orbital greatly facilitates the redox communication between metals in the ytterbocene complexes.

The separation between the bridging-ligand based waves ($\Delta(E_{1/2})[L_1 - L_2]$ in Table 3) for the bimetallic complexes should still reflect principally the spin-pairing energy in the ligand-based LUMO found in the free ligand data, but include some perturbation from the influence of the coordinating metal ion(s).[23] It is clear from the data in Table 3 that here, too, complex **1** exhibits the greatest perturbation; the $\Delta(E_{1/2})[L_1 - L_2]$ value for the complex is nearly twice that found for the free ligand. The perturbations in $\Delta(E_{1/2})[L_1 - L_2]$ for **2** and **3** are much smaller and in the opposite direction (i.e., $\Delta(E_{1/2})[L_1 - L_2]$ for the complex is smaller than that for the free ligand). The comparison with the corresponding bimetallic ruthenium complexes is less informative for these ligand-based processes, although it is notable that there is reportedly no separation in the ligand-based oxidation processes for dtb in the ruthenium system. The possibility of spatial localization of the electrons into degenerate or nearly degenerate π^* orbitals in these bridging ligands cannot be discounted, particularly for qtp and dtb, since they in principle possess rotational degrees of freedom between the tpy fragments that could disrupt the delocalization of the LUMO across the entire ligand span. In such a case, the separation between ligand-based oxidation waves would not reflect the spin-pairing energy, but would instead provide a measure of the energetic separation between the π^* orbital energies. The lack of structurally characterized qtp and dtb systems in the literature make it difficult to confirm conformational changes due to oxidation state changes in the solid state. However, we have no direct evidence for this phenomenon in the bimetallic ytterbocene systems, and the magnetic data are most consistent with the spin-paired $(\pi^*)^2$ configuration in the neutral complexes.

Optical Spectroscopy. UV−visible-near-IR electronic absorption spectral data have been obtained for complexes **1**−**4** as neutral species, monocationic species, and for **1**−**3** as dicationic species. The spectra are presented in Figure 4. Data for **1** and **4** as neutral species were reported previously[5] but are reproduced here for comparison with the data for the other complexes. Data were also obtained for the singly reduced free ligand radical anions and are included in Figure 4 D for comparison. Note that the spectra for **4** and $[\mathbf{4}]^+$ have been grouped with those of the bimetallic complexes to reflect common oxidation states on the ligand instead of overall charge on the complex because this is most representative of the nature of the electronic states available in these systems. The complexity of these spectral data precludes a detailed assignment of all observed electronic transitions. Instead, we focus here on the common features between and among the complexes in the different oxidation states and concentrate on aspects that might reflect the electronic structure and the degree to which the metal centers in the bimetallic complexes interact.

The working hypothesis in the consideration of all these spectral data is that the neutral bimetallic complexes are dominated at room temperature by a species possessing the ground-state electronic configuration $[(f)^{13}-(\pi^*)^2-(f)^{13}]$. This hypothesis is based on interpretations of magnetic susceptibility and NMR data presented here, and is consistent with the electronic configuration proposed previously by Andersen and co-workers for analogous bimetallic ytterbocene complexes.[3] The spectral data for these neutral bimetallic complexes exhibit intense bands throughout the entire spectral region. The UV−visible region of the spectrum for **2** and **3** is quite similar. This same region for **1** reveals structurally similar spectral features that appear to be shifted to lower energy by ~10 000 cm^{-1}. The spectra for all three complexes exhibit a fairly narrow, intense, vibronically structured band in the NIR ($E_{00} \approx 10\,000$ cm^{-1}). Finally, all three spectra possess several much weaker bands on the low-energy tail of this NIR band.

All of the intense bands in the spectra of **1**−**3** are ascribed to fully allowed bridging-ligand localized transitions between the occupied π and π^* levels and lower lying unoccupied π^* levels. Unfortunately, we were unable to chemically prepare dianionic species of the free ligands to obtain spectral data for comparison, and published spectral data for doubly reduced polypyridyl ligands are only available for bipyridine.[27] However, there are literature reports of dianions of porphyrin-like ligands for which very similar spectral results are obtained.[28] In particular, the lowest energy band of the dianionic ligands ($E_{00} \approx 10\,000$ cm^{-1}) is attributed to a transition in which an electron is promoted from the doubly occupied π^* orbital to the next lowest-lying π^* orbital. Such a transition would not be expected to result in substantial structural distortions because it is antibonding-to-antibonding in nature and the Franck−Condon factors are expected to be small. This expectation is consistent with the rather narrow line widths found in the ~10 000 cm^{-1} bands for complexes **1**−**3**; the line widths suggest that only 1−2 vibronic lines contribute to the profiles. This observation of energetically and structurally similar bands in the spectra of **1**−**3** supports the $(\pi^*)^2$ electronic configuration assignment in these neutral complexes. The presence of $4f^{13}$ metal centers in these neutral species might be expected to engender metal-localized f−f transitions in these spectral data that should be most informative with respect to metal−metal interactions. Unfortunately, these transitions are known to be fairly weak and lie at ~10 000 cm^{-1} (vide infra) and would therefore be buried underneath the much more intense $\pi^*-\pi^*$ transition in this region. This same phenomenon has been observed and described previously for monometallic polypyridine adducts of ytterbocene.[1]

The optical spectra for $[\mathbf{1}]^+$, $[\mathbf{2}]^+$, and $[\mathbf{3}]^+$ along with that of the neutral complex of **1** are presented in Figure 4B. As with the data for the neutral bimetallic species, there are many similarities in the spectra of the cationic bimetallic complexes throughout the entire spectral range. Generally, the intensities and line widths in the spectra for all species in this comparison

(27) Konig, E.; Kremer, S. *Chem. Phys. Lett.* **1970**, *5*, 87.
(28) (a) Bachmann, R.; Gerson, F.; Gescheidt, G.; Vogel, E. *J. Am. Chem. Soc.* **1993**, *115*, 10286. (b) Bachmann, R.; Gerson, F.; Gescheidt, G.; Vogel, E. *J. Am. Chem. Soc.* **1992**, *114*, 10855.

indicate fully allowed molecular (as opposed to ligand-field or metal-localized) transitions. The vibronic structure seen for most of the bands in these spectra is consistent with transitions having a large Franck−Condon factor derived from a substantial change in the bonding character in the ligand between ground and excited states (e.g., bonding ↔ antibonding).

There are numerous examples in the literature of electronic spectral data for both uncomplexed [27,29] and transition-metal complexed singly reduced polypyridyl ligands.[30,31] These spectral data universally exhibit vibronically resolved bands attributed to ligand-localized $\pi-\pi^*$ and $\pi^*-\pi^*$ transitions in the energy window between ∼15 000−5000 cm^{-1}. The intensities in these ligand radical anion bands, however, are typically less than ∼5000 $M^{-1}cm^{-1}$ presumably because these transitions are not rigorously electric-dipole allowed.[27] As illustrated in Figure 4D, transitions are observed for the radical anions of the uncomplexed ligands under investigation here, but the extinction coefficients for these lowest energy bands are substantially lower than those of the lowest energy bands observed for the corresponding cationic complexes (Figure 4B). Thus, we assign the lowest energy bands observed for these cationic complexes (and the neutral **4**), because of the greater intensities and more pronounced vibronic features, to charge transfer transitions, with the ligand radical anion-based transitions (similar to those seen for the free ligand radical anions, Figure 4 D) lying to slightly higher energy and/or buried beneath the more intense charge-tranfer bands.

Charge-transfer transitions have been observed previously for neutral monometallic ytterbocene complexes, and described as ligand-to-metal in nature arising from promotion of the π^* electron on the polypyridyl ligand to the metal f orbital manifold to achieve the $[(f)^{14}-(\pi^*)^0]$ configuration.[1] This assignment is favored for these cationic bimetallic species as well. The lowest energy spectral bands observed for $[\mathbf{1}]^+$ do not have the same general characteristics as those of the other complexes shown in Figure 4B, and in fact, the lowest energy band observed for $[\mathbf{1}]^+$ looks nearly identical to that seen in the tppz radical anion spectrum (Figure 4 D). Inasmuch as nearly all of the spectral bands for tppz and its complexes in all oxidation states seem to be shifted to lower energy, it seems probable that the ligand-to-metal charge-transfer transition in $[\mathbf{1}]^+$ lies to lower energy than we can resolve in solution with our instrumentation. These cationic bimetallic complexes should also possess f−f transitions that could provide some insight into metal−metal interactions in this oxidation state. However, these bands should still occur at ∼10 000 cm^{-1}, and this spectral window continues to be dominated by the charge-transfer and ligand-radical anion-based transitions that have significantly higher molar extinction coefficients.

The final set of spectral data is that for the dicationic bimetallic complexes and the monocation of **4** (Figure 4 C). These spectral data are significantly simplified relative to the neutral and cationic complex data because these species no longer possess electrons in polypyridyl-based π^* orbitals that engender the intense transitions throughout the visible and NIR. The most intense resolved transitions for these complexes, at energies greater than ∼28 000 cm^{-1} (> ∼22 000 cm^{-1} for $[\mathbf{1}]^{2+}$) are assigned to $\pi-\pi^*$ transitions localized on the polypyridyl and Cp* ligands. There are two additional unique features common to the spectra of all these dicationic species (and $[\mathbf{4}]^+$). The first is the broad set of bands with a center of gravity that occurs in the mid-visible region for $[\mathbf{4}]^+$ (E_{max} = 23 725 cm^{-1}), $[\mathbf{2}]^{2+}$ (20 890 cm^{-1}), and $[\mathbf{3}]^{2+}$ (22 690 cm^{-1}), but which shifts to much lower energy for $[\mathbf{1}]^{2+}$ (16 480 cm^{-1}). There are at least two poorly resolved bands in each set. The more intense of these bands is assigned to a polypyridyl ligand (π)-to-metal (4f) charge-transfer transition on the basis of detailed resonance Raman data for $[\mathbf{4}]^+$ presented elsewhere[5b] and by analogy to the spectrum of oxidized (d^5) transition-metal polypyridyl complexes (e.g., $[Ru(bpy)_3]^{3+}$).[31,32] The less intense band(s) in this region are assigned to the related Cp* ligand (π)-to-metal (4f) charge transfer transition(s). This assignment is based on comparison to the spectra of many structurally related monometallic ytterbocene complexes (e.g., Cp^*_3Yb and $Cp^*_3Yb(L)$; L = THF, PEt_3, etc.).[33] The second new feature for these dicationic species (and $[\mathbf{4}]^+$) is the emergence of the f−f transitions deriving from the $4f^{13}$ electronic configuration on the two ytterbium (one for $[\mathbf{4}]^+$) centers (Figure 4 C (inset)). As expected on the basis of data from other Yb(III) complexes, these bands are centered at ∼10 000 cm^{-1}, they are quite narrow, and they have much lower oscillator strengths consistent with the Laporte parity-forbidden nature of the transitions. Note that the putative ligand-to-metal charge-transfer transitions for $[\mathbf{1}]^{2+}$ occur at such low energy that these bands tail well into the f−f region. However, for the other complexes the f−f bands are well resolved from all other electronic transitions.

To examine in greater detail the comparative properties of the f−f bands in these four species, the contribution to the f−f region from the sloping low-energy tail of the charge-transfer bands in $[\mathbf{1}]^{2+}$ was eliminated by fitting the charge-transfer band envelope to a Gaussian profile and subtracting this profile from the f−f band data. Figure 5 shows the rather striking energy and intensity comparison of the f−f spectral region for the four complexes. Note, in particular, the overall similarity in the spectra between $[\mathbf{4}]^+$, $[\mathbf{2}]^{2+}$, and $[\mathbf{3}]^{2+}$ in peak positions and intensities. In contrast, there is a decided difference in the positions and intensities of the bands in $[\mathbf{1}]^{2+}$. To quantify this comparison, the spectra in this region for all four species were fit using Voigt functions.[34] (Attempts to fit the spectra with either pure Gaussian or pure Lorentzian profiles were totally inadequate. Examples of the quality of the spectral fitting are provided in the Supporting Information.) The metrical results from this exercise are provided in Table 4.

If the metal centers in these dicationic bimetallic species were to exhibit strong electronic interaction, one might anticipate some substantial perturbation to the energies and intensities of the f−f bands relative to those found in the monometallic species. In contrast, if the metal centers are totally noninteracting, one would expect very similar spectral profiles having twice the intensity in the bimetallic systems as seen in the bands of $[\mathbf{4}]^+$. The unique f−f spectral data for $[\mathbf{1}]^{2+}$ clearly

(29) Braterman, P. S.; Song, J.-I. *J. Org. Chem.* **1991**, *56*, 4678.
(30) (a) Heath, G. A.; Yellowlees, L. J.; Braterman, P. S. *Chem. Phys. Lett.* **1982**, *92*, 646. (b) Tait, C. D. M., D. B.; Donohoe, R. J.; DeArmond, M. K.; Hanck, K. W.; Wertz, D. W. *J. Phys. Chem.* **1986**, *90*, 1766. (c) Jones, S. W.; Vrana, L. M.; Brewer, K. J. *J. Organomet. Chem.* **1998**, *554*, 29.
(31) Braterman, P. S.; Song, J.-I.; Peacock, R. D. *Spectrochim. Acta* **1992**, *48A*, 899.
(32) (a) Nazeeruddin, M. K.; Zakeeruddin, S. M.; Kalyanasundaram, K. J. *J. Phys. Chem.* **1993**, *97*, 9607. (b) Bergkamp, M. A.; Butlich, P.; Netrel, T. L.; Sutin, N. J. *J. Phys. Chem.* **1983**, *87*, 3877. (c) Bryant, G. M. F., J. E. *Aust. J. Chem.* **1971**, *24*, 275.
(33) Schlesener, C. J.; Ellis, A. B. *Organometallics* **1983**, *2*, 529.
(34) Armstrong, B. H. *J. Quant. Spectrosc. Radiat. Transfer* **1967**, *7*, 61.

Table 4. Summary of f−f Transition Parameters from NIR Spectra of Cationic Ytterbocene Complexes[a,b]

	band I		band II		band III		band IV	
complex	energy (cm^{-1})	integrated intensity	energy (cm^{-1})	integrated intensity	energy (cm^{-1})	integrated intensity	energy (cm^{-1})	integrated intensity
[4]$^{+}$	10273	6370	10135	2510	9987	3950	9855	1930
[2]$^{2+}$	10271	9760	10127	5580	9981	8700	9847	3130
[3]$^{2+}$	10267	6830	10138	5090	9978	6710	9849	2030
[1]$^{2+}$	10244	10550	10061	4980	9884	21170	9802	18770

[a] See Figure 5 for identification of bands. [b] Integrated intensities (arbitrary units) are derived from the unconstrained Voigt profile fits of the spectra; see text for details.

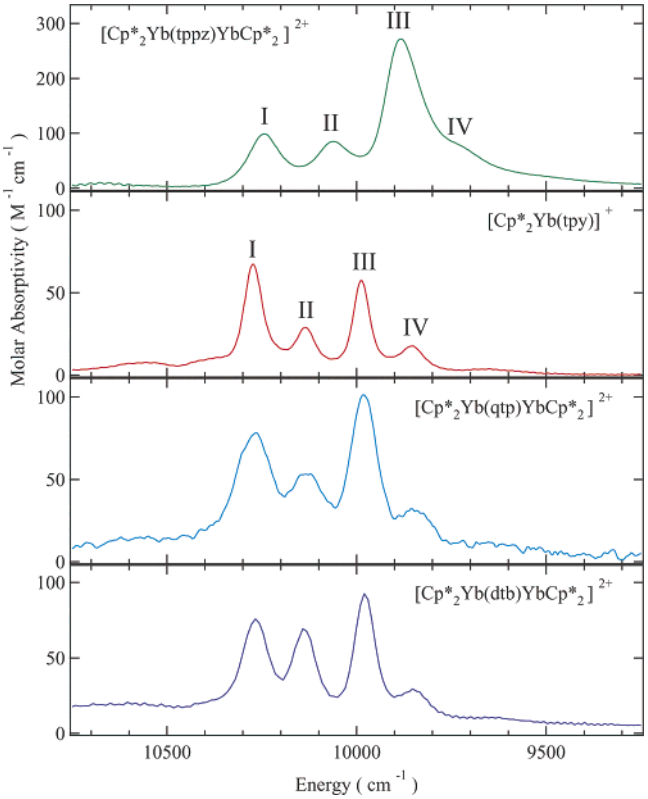

Figure 5. Near-IR spectral data for fully oxidized ytterbocene complexes in CH_2Cl_2.

demonstrate that this system falls within the regime of strong perturbations demonstrating significant metal−metal electronic interaction across this shortest of metal−metal distances. As the data for the four main bands illustrate (Table 4), the intensities in the bands for **[2]**$^{2+}$ and **[3]**$^{2+}$ are ∼2× that of **[4]**$^{+}$. However, careful consideration of the individual line shapes in the spectrum of **[2]**$^{2+}$ reveals that each principal band is in fact two very closely spaced, narrower bands similar to those seen in **[4]**$^{+}$, but unresolvable at the this level of spectral resolution. This interpretation is consistent with a very small metal−metal electronic interaction in **[2]**$^{2+}$ that leads to a small, but noticeable splitting of the f−f states, and an essentially negligible metal−metal interaction over the larger bridging ligand separation in **[3]**$^{2+}$ such that the intensities approximately double without individual band splittings. No attempts were made to fit the spectrum of either **[2]**$^{2+}$ or **[3]**$^{2+}$ with an extra set of four bands as suggested by this interpretation, since this exercise would certainly lead to improved fits but could not be justified on the basis of the observed resolution or density of data points.

Summary and Conclusions.

The optical spectroscopic results for these ytterbocene complexes demonstrate that the spectra are dominated (for all systems except the dicationic species and **[4]**$^{+}$) by the one- or two-electron reduced polypyridyl ligands. A further illustration of the importance of these reduced ligands in dictating the UV−visible-NIR landscape is provided by comparison of the bimetallic tppz and monometallic tpy complexes of Cp^*_2Sm with those of Cp^*_2Yb (see Supporting Information). There is a nearly exact match of energies and intensities of all bands between these two metallocene adducts. The optical data also point to the unique character of the tppz bridging ligand in comparison to the other polypyridyl ligands studied here. For all categories of electronic transition (ligand-based, charge-transfer, and f−f) in all oxidation states the data for the tppz species differ from the otherwise similar behavior seen for **4**, **2**, and **3**. This is, in part, a reflection of the shorter metal−metal separation for this bridging ligand and the change in the relative energies of the ligand HOMO and LUMO in comparison to those of the other polypyridyl ligands.

Unfortunately, while the electrochemical data suggest a substantial (several hundred mV) electronic interaction between the metal centers for the neutral bimetallic complexes for which there are two π^* electrons on the bridging ligand, the critical optical data are obscured with respect to this electronic interaction because of the dominance of the ligand-based transitions that mask the f−f bands for both the neutral and monocationic complexes. Nonetheless, the optical data associated with the dicationic bimetallic species do provide evidence from the f−f bands for a metal−metal electronic interaction (**[1]**$^{2+}$ > **[2]**$^{2+}$ > **[3]**$^{2+}$). However, the magnitude of the electronic interaction in the dicationic species is clearly much smaller than that of the neutral redox congeners. This observation highlights the apparent importance of the antibonding electrons on the bridging ligand to intensifying the metal−metal electronic communication.

The magnetic behavior of these complexes appears to be quite sensitive toward the nature of the bridging ligand. Differences in the data collected for **2** in relation to complexes **1** and **3** illustrate this sensitivity. The difference in behavior appears to be consistent with Class 3 or antiferromagnetic exchange coupling observed previously by Andersen and co-workers,[3] inasmuch as the reduction potentials for free qtp are substantially more negative than those of the other bridging ligands. The metal−metal separation, redox potentials and nature of the LUMO appear to be key aspects that dictate the magnetic properties. Future studies will focus on quantifying the extent of the Yb−Yb magnetic coupling and electronic communication through the application of magnetic circular dichroism (MCD)

in an attempt to isolate the f−f spectral bands from the more intense ligand-localized bands.

Acknowledgment. Funding for this work was provided by Los Alamos National Laboratory's Laboratory Directed Research and Development program and by the U. S. Department of Energy, Office of Basic Energy Sciences under the auspices of the Heavy Element Chemistry program. All work was performed at Los Alamos National Laboratory under contract with the University of California (Contract No. W-7405-ENG-36), except for the collection of the X-ray data for **[4]**$^+$. We thank Mark A. Rodriguez of Sandia National Laboratory, Albuquerque, New Mexico for the collection of the X-ray data for **[4]**$^+$. C.N.C., R.E.D., J.M.V., E.J.S., E.D.B., and A.E.M. thank the Seaborg Institute for postdoctoral and student fellowships. C.J.K. thanks the U.S. Intelligence Community for a postdoctoral fellowship.

Supporting Information Available: Full crystallographic details for [**1**]$^+$, [**4**]$^+$ and for $[(C_5Me_4Et)_2Yb]_2$qtp are available as CIF files, plots of χT vs T for complexes [**1**]$^{0/+/2+}$, [**2**]$^{0/+/2+}$, [**2**]$^{0/+/2+}$, molecular orbital output of the bridging ligands, cyclic voltammograms of [**1**]$^{-/0/+/2+}$, fits of the f−f transitions of [**1**]$^{2+}$and [**3**]$^{2+}$, and synthetic/spectroscopic details of Cp^*_2Sm(tpy) and Cp^*_2Sm(tppz)SmCp^*_2 are also available. This material is available free of charge via the Internet at http://pubs.acs.org.

JA058667E